Journal of Molecular Liquids 389 (2023) 122828

Contents lists available at ScienceDirect

Journal of Molecular Liquids

journal homepage: www.elsevier.com/locate/molliq

Conformational flexibility of spermidine^{3+} interacting with DNA double helix

Sergiy Perepelytsya [a,b,*], Tudor Vasiliu [c,d], Aatto Laaksonen [c,e,f,g,h], Leon De Villiers Engelbrecht [h], Giuseppe Brancato [i,j], Francesca Mocci [h,*]

[a] Bogolyubov Institute for Theoretical Physics of the National Academy of Sciences of Ukraine, Kyiv 03143, Ukraine
[b] National University of Kyiv-Mohyla Academy, Kyiv 04070, Ukraine
[c] Center of Advanced Research in Bionanoconjugates and Biopolymers, "Petru Poni" Institute of Macromolecular Chemistry, Iasi 700487, Romania
[d] The Research Institute of the University of Bucharest (ICUB), 90 Sos. Panduri, 050663 Bucharest, Romania
[e] Department of Materials and Environmental Chemistry, Division of Physical Chemistry, Arrhenius Laboratory, Stockholm University, 106 91 Stockholm, Sweden
[f] State Key Laboratory of Materials-Oriented and Chemical Engineering, Nanjing Tech University, 210009 Nanjing, PR China
[g] Department of Engineering Sciences and Mathematics, Division of Energy Science, Luleå University of Technology, 97187 Luleå, Sweden
[h] Department of Chemical and Geological Sciences, University of Cagliari, 09042 Monserrato, Italy
[i] Scuola Normale Superiore and CSGI, Piazza dei Cavalieri 7, I-56126 Pisa, Italy
[j] Istituto Nazionale di Fisica Nucleare (INFN) sezione di Pisa, Largo Bruno Pontecorvo 3, I-56127 Pisa, Italy

ARTICLE INFO

Keywords:
Polyamine
Spermidine^{3+}
DNA double helix
Molecular dynamics
Conformation
Dihedral angle

ABSTRACT

Natural polyamines play a key role in many biological processes, particularly in the stabilization of DNA double helix structure in the cell nucleus. Among others, the conformational flexibility of polyamines, such as spermidine, is an essential property for the formation of complexes with DNA. Yet, the characterization of the conformational space of polyamines has not been fully elucidated. Using atomistic molecular dynamics (MD) simulations, we present a detailed study of the conformational space of spermidine^{3+} both in solution and in interaction with DNA. We have identified more than 2000 distinct conformations, which can be grouped into seven modes. Notably, the relative population of these modes is highly affected by the interaction of spermidine^{3+} with DNA, thus representing a fingerprint of complex formation. In particular, three of the seven dihedral angles of spermidine^{3+} are predominantly in *trans* conformation (with or without DNA), while the other four dihedral angles are observed to switch between *trans*, *gauche*$^+$ and *gauche*$^-$. The preference between the latter conformational states was analyzed in terms of the distinct energy contributions composing the potential energy. Overall, our results shed light on the conformational equilibrium and dynamics of spermidine^{3+}, which in turn is important for understanding the nature of its interaction with DNA.

1. Introduction

The DNA double helix is a highly charged polyelectrolyte due to the negatively charged phosphate groups in the macromolecule backbone. In the cell nucleus, such electric charges are neutralized by positively charged protein residues, metal ions (e.g., K^+ and Mg^{2+}), and the natural polyamines, such as putrescine^{2+}, spermidine^{3+}, and spermine^{4+} [1]. The interactions of small and mobile metal ions with the DNA double helix are widely described in the literature [2–10], while the DNA-polyamine interactions, despite their great interest in stabilizing the DNA structure and involvement in many cellular processes, are still far from being completely characterized structurally and dynamically. Natural polyamines are topologically linear molecules that can adopt a great variety of conformations. This conformational flexibility plays a key role in DNA-polyamine interaction, [11–13] and its characterization is therefore relevant for better understanding many biological processes, from the condensation of DNA to the protection against oxidation. Yet, the detailed investigation of the complex conformational space of the flexible polyamines represents a challenge for both theory and experiments.

In competition with other counterions, the positively charged polyamines interact strongly with the negatively charged DNA backbone, exhibiting different binding modes [12,14–19]. In particular, spermidine^{3+} can orient itself parallel or orthogonal to the helical axis of

* Corresponding authors.
E-mail addresses: perepelytsya@bitp.kiev.ua (S. Perepelytsya), fmocci@unica.it (F. Mocci).

https://doi.org/10.1016/j.molliq.2023.122828
Received 5 May 2023; Received in revised form 31 July 2023; Accepted 11 August 2023
Available online 12 August 2023

DNA, and it can be found located both inside and outside the minor or major groove [14–18]. Polyamine molecules can also bridge two or more phosphate groups belonging to the same or different strands of the double helix, or even to different DNA macromolecules [13,18]. These electrostatic mediated bridges between different segments of DNA allow to organize and compact the genome, as well as to promote the chromosome condensation during cell division [21–23]. Polyamines can also interact with other molecules like proteins and RNA, and in this way participate in a great variety of cellular processes. Depending on their length and conformational degrees of freedom, the three natural polyamines can show slightly different binding modes and roles in biological processes. Also, these phenomena, related with the formation of the polyamine-mediated cross-links, occur when their concentration is sufficiently high [12–14,20,21].

The structure and dynamics of the DNA-polyamine complexes influence the elastic properties of the double helix, determines DNA condensation, and induces conformational transformations [14,18,22,23]. Previous molecular dynamics (MD) studies of DNA interactions with putrescine^{2+}, spermidine^{3+}, and spermine^{4+} have shown that the stability of the DNA-polyamine complexes increases with increasing polyamine charge [19]. The preferred polyamines binding sites are the DNA grooves, where they display the longest residence times [15,17,19]. Experimental studies [24,25] and MD simulations [11] have revealed that some sequence specificity in the interactions with the DNA can be observed related to the width of the grooves and correlated to the natural narrowing of the minor groove in the AT-rich nucleotide regions. Those polyamines residing completely inside the narrow minor grooves show residence times of hundreds of nanoseconds [11]. At the same time, simulations at high spermidine^{3+} concentrations have shown that polyamines become only partially inserted into the deeper regions of the grooves while less affected by the width of the groove [12]. In the case of partial localization of spermidine in the minor groove, its conformation can be highly variable from highly bent to completely stretched linear structure.

Clearly, the conformational flexibility of spermidine^{3+} is of paramount importance for determining the interaction modes with the DNA double helix [12,13]. Indeed, spermidine is highly flexible since it has seven single rotatable bonds along the molecule backbone. For each rotatable bond, there are three distinct energy minima (i.e., *trans*, *gauche*$^{+}$, and *gauche*$^{-}$). Taking this into consideration, the conformational space of spermidine^{3+} may count up to 3^7 different conformations. However, as the experimental data show [26,27], the energy difference between the *trans* and *gauche* states depends on the considered dihedral angle, with some of them preferring the *trans* state, while others the *gauche*$^{+/-}$. In this context, MD simulations are a powerful tool to provide a detailed classification of the conformational landscape of polyamines and its role in biological processes, which is still missing.

In the present work, we have systematically investigated the conformational preferences of spermidine^{3+} in aqueous solution, both in the absence and presence of a DNA double helix with the aim to identify the most populated conformations of this polyamine. This paper is organized as follows. Simulation details are described in Sec. 2. In the Results (Sec. 3), the conformational states of spermidine^{3+} are classified by analyzing the end-to-end distance together with the dihedral angle distributions. The changes in the conformational preferences of spermidine^{3+} interacting with the DNA double helix are carefully analyzed and the most probable conformations of spermidine^{3+} in different regions around the double helix are described. Conclusions and

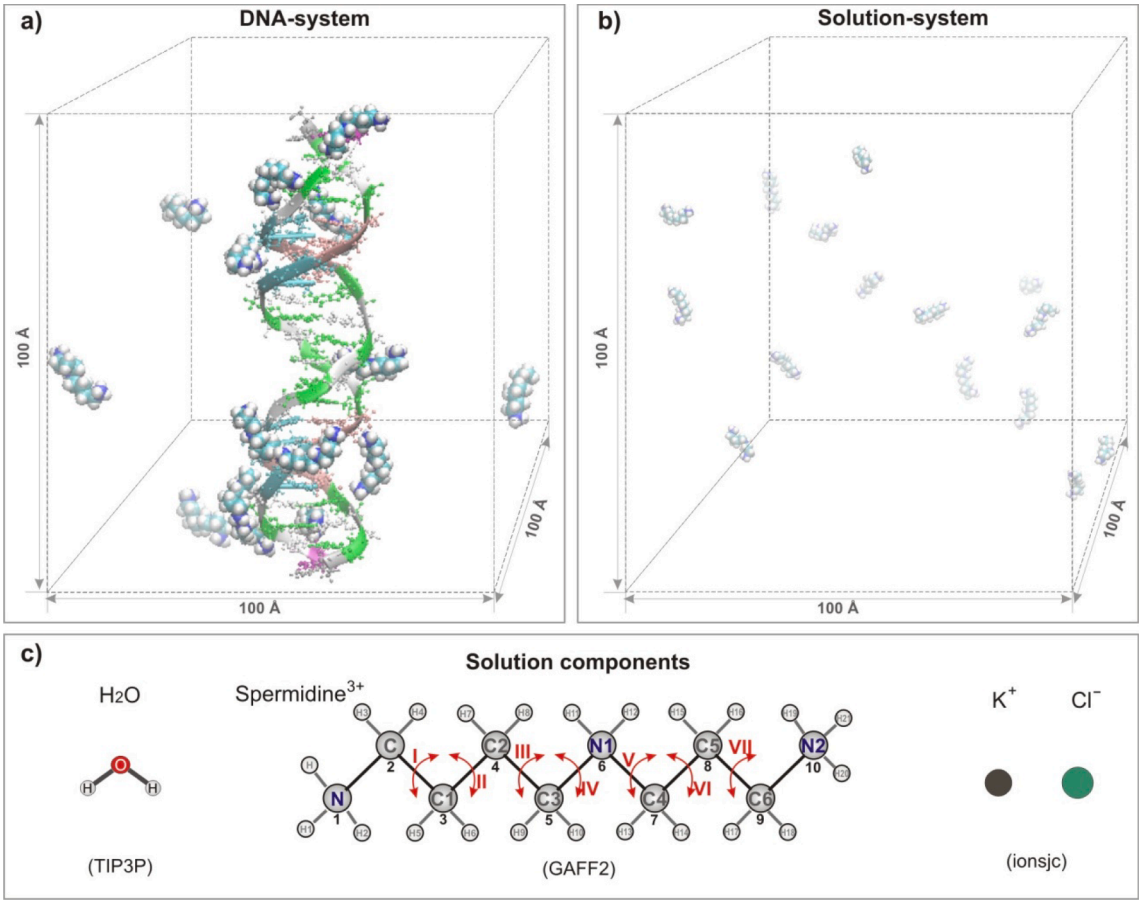

Fig. 1. Simulated systems. **a)** DNA- system. **b)** Solution- system. In **a)** and **b),** water molecules are not shown for clarity. **c)** The components of the solution: Structure of spermidine^{3+}, with name and numbering of the atoms, and labels (Roman numbers) used for the dihedral angles indicated with red arrows in the molecule backbone.

perspectives are provided in Sec. 4.

2. Methods

2.1. Simulation details

Two systems have been modeled using MD simulations (Fig. 1). The first one consists of 15 spermidine^{3+} molecules, charge-neutralized with chloride ions, dissolved in a water solution with KCl at 0.15 M concentration. It will be indicated below as "solution-system". The second system differs from the first one by having, in addition to 15 spermidine^{3+} molecules in a water solution at 0.15 M KCl concentration, a DNA double helix with nucleotide sequence d(CGCGAATTCGCGCGAATTCGCG). It will be indicated in the following as "DNA-system". For each system, the numbers of molecules are reported in Table 1. The edge lengths/volume of the cubic box were initially 100 Å x 100 Å x 100 Å.

The DNA oligomer was built based on the Arnott *B*-DNA canonical structure using the nucleic acid builder (NAB) tool included in the Amber 18 package [28], while the spermidine^{3+} structure was prepared using Avogadro [29,30]. The bonded and non-bonded parameters were obtained from the AMBER BSC1 DNA force field [31] for DNA, and for spermidine^{3+}the GAFF2 version of the Generalized Amber Force Field [32], distributed with Amber 18, was used. The TIP3P model was used for water molecules [33], while K^+ and Cl^- ions were modeled using the ionsjc parameter set [34] for TIP3P.

All simulations were performed using the GROMACS 2018 simulation package [35]. The Nosé-Hoover thermostat [36,37] was used to control the temperature at 298 K, while the Parrinello-Rahman barostat [38] was used to control the pressure, which was set at 1 bar. The lengths of all bonds with hydrogen atoms were constrained using the LINCS algorithm [39]. The long-range electrostatic interactions were treated using the smooth particle mesh Ewald method [40]. The switching and cut-off distances for the long-range interactions were both at 10 Å, respectively, and the Fourier spacing was 1.2 Å.

After the systems were built, we performed energy minimization to remove any overlap between atoms. After energy minimization, the MD simulation for the solution-system was started (time = 0) setting the temperature at 300 K by randomly distributing the corresponding velocities according to the Maxwell Boltzmann distribution. Differently, in the case of the DNA-system, the initial 10 ns of the MD simulations were performed applying a 1000 kJ/(mol·nm^2) positional restraint on the entire DNA molecule, to allow first the equilibration of the DNA solvating environment and to avoid any distortion in the DNA conformation. After these first 10 ns, all restraints were removed and the unrestrained MD simulation was started (time = 0).

For the DNA-system, multiple simulation trajectories (A, B, C, D, and E) were generated. The systems were built by placing the DNA in the middle of the simulation box, and after that the spermidine was distributed randomly at a minimum distance of 5 Å from the DNA. The simulations were repeated three times, each time redistributing randomly the spermidine molecules. This protocol was chosen to avoid that the initial placement could bias the results concerning the mode of interaction with DNA. Each of the three MD simulations had a length of the trajectory of ca. 1000–1100 ns and two of them were extended 400 ns more, to check if the system was equilibrated enough to provide reliable result or if the behavior of spermidine in this extended trajectory is significantly different from the 1μs trajectories. Trajectory A had a length of ~ 1000 ns and the trajectories B and C ~ 1100 ns. The trajectories D and E are the above-mentioned prolongations of the trajectory B and C by ~ 400 ns. The first 250 ns of the trajectories A-C were considered as equilibration and excluded from the analysis. This choice was determined by the large variation observed in the number of molecules interacting with the major groove and with the minor groove/phosphate (see Figure S1), during the initial 150–250 ns of the trajectories.

In the solution-system, the distribution of the end-to-end distances of the polyamines reaches equilibrium within the first tens of nanoseconds of the simulation trajectory, with all the molecules having the same distribution. The length of the simulation trajectory was 1000 ns. In the analysis, the first 200 ns were neglected. This time was more than enough to reach equilibrium, as demonstrated by the individual and global end-to-end distances calculated between 100 ns and 200 ns, reported in Figure S2. The analysis and visualization of the simulation trajectories were carried out using the VMD software package [41].

Table 1
Simulation box details.

System name	Nr. of spermidine^{3+}	Nr. of DNA	Nr. of waters	K^+/Cl^-
solution-system	15	0	31,888	90/135
DNA-system	15	1	31,930	90/93

2.2. Characteristics of spermidine^{3+} structure

The structure of spermidine^{3+} consists of 10 "heavy" atoms (carbon and nitrogen) in the molecule backbone, to which are bonded 22 hydrogen atoms. The atoms are connected by single bonds (Fig. 1d). The total number of chemical bonds in one spermidine^{3+} molecule is 31. In the MD simulations, the interactions between the atoms of spermidine^{3+} are determined by the potential energy of intramolecular and intermolecular interactions. The intramolecular interactions consist of the potential energy of bonds, valence angles, and dihedral angles, while intermolecular interactions are presented by the electrostatic and van der Waals interactions. The explicit form of the potential energy and the values of electrostatic charge for each atom are shown in the Supplemental Materials (formula S1 and Table S1).

In our MD simulations, the bonds between hydrogen atoms and heavy atom are fixed at the equilibrium positions by the LINCS algorithm [39]. Therefore, the bond energy of the polyamine molecule is determined by $N_B = 9$ chemical bonds between atoms in the polyamine backbone. Due to the same reasons the energy of valence angles is determined by $N_A = 8$ valence angles between the heavy atoms in spermidine^{3+} backbone. The number of dihedral angles making the contribution to the energy in equation (S1) is a sum of 7 dihedral angles formed by the atoms in the backbone and 32 dihedral angles involving hydrogen atoms; thus, $N_D = 39$.

The contribution to the nonbonded interactions energy terms in equation (S1) may be divided into two categories. In the first category are the interactions with the atoms that are not part of polyamine molecules (water molecules, ions, DNA atoms). The interactions of the atoms of spermidine^{3+} between each other belong to the second category. Note that in the present MD simulations the nonbonded intramolecular interactions between atoms separated by only 3 bonds (1–4 interactions) are reduced by a factor 1.2 and are not considered for atoms separated by <3 bonds.

To determine which intrinsic interactions are driving the conformational preferences of spermidine^{3+}, we analyze first the distributions of the backbone bond lengths together with the valence and dihedral angles in the solution-system. The probability distributions for these structural parameters were fitted to Gaussians (Figure S5), as discussed in detail in Section S3 of the Supplemental Materials. The analysis shows that the changes in the molecular structure during the MD simulation mainly involve the dihedral angles. The valence bonds and angles are rather rigid and fluctuate very little around the equilibrium values of the force field parameters. Therefore, in the following analysis, only the backbone dihedral angles of the spermidine^{3+} are considered.

3. Results

3.1. End-to-end distance analysis of spermidine^{3+}

The conformational space of linear molecules is usually

characterized by the distance between the two ends [42]. In the case of long molecules, the mean value of end-to-end distance (EED) characterizes the degree of compaction of the molecule in solution. In the case of relatively short molecules, EED is directly related to the conformational state of the molecule, and, in the present work, it is used to characterize the spermidine^{3+} conformation. EEDs were calculated for each polyamine molecule every 1000 steps of the simulation trajectories of the solution-system and DNA-system. Using the calculated values, the probability density distribution of the EED was built separately for each spermidine^{3+} molecule of the system (Figure S4 for the DNA-system, and Figure S5 for the solution-system). The results for the DNA-systems show that the EED distributions have 7 characteristic peaks within the range 3 Å to 12 Å (Figure S2f). Based on the observed peaks, the conformation of spermidine^{3+} can be divided into 7 families of conformations. The distribution among the modes, as shown in Figure S4, is not the same for each spermidine^{3+}: depending on the molecule, some peaks can be prominent and some very weak or even absent, as a result of the interaction with the DNA double helix. Differently, in the solution-system the EED distribution is rather similar for all polyamines in the system (Figure S5). On the overall, this indicates that the interactions of the polyamines with the charged atoms of DNA stabilize the conformational state for a relatively long time, and consequently even in trajectories longer than 1 μs as those used here, the polyamine cannot sample the entire conformational space. In the present work, the EED probability density distributions for spermidine^{3+} and the observed peaks are called conformational "spectra" and conformational "modes", respectively, by the analogy with modes in vibrational spectra.

In the following, the averaged conformational spectra of spermidine^{3+} molecules is analyzed. The averaged conformational spectrum for each trajectory has been calculated by averaging the spectra of each polyamine molecule in the system. In the case of the DNA-system, the averaged conformational spectrum was obtained for each simulation trajectory (A, B, C, D and E); then, the obtained averaged conformational spectra for each conformational trajectory were averaged to obtain the final conformational spectra. The conformational spectra averaged over all polyamines and over all simulation trajectories for DNA-system, are shown in Fig. 2a, and those for the solution-system in Fig. 2b. The error bars describe the range of deviations of each particular spectrum from the averaged curve.

The results for the DNA-systems in trajectories A-E (see Figure S5f), show that all conformational spectra are characterized by 7 peaks that may have slightly different intensity, but the position of each peak is about the same. The shape of the spectrum is qualitatively the same, in the case of different simulation trajectories. To analyze the conformational changes of the spermidine^{3+} molecule the mean spectra of all trajectories were averaged and then fitted by the 7 Gaussian functions. The detailed parameters of Gaussians are shown in the Section S3 of Supplemental Materials (Table S3).

The conformational state of spermidine^{3+} is essentially different in different regions of the spectra. Taking into consideration the intensities of the modes (Fig. 2), the conformational spectra of spermidine^{3+} molecule may be conditionally divided into three regions: bent (<7.3 Å), intermediate (from 7.3 Å to 10.2 Å) and stretched (>10.2 Å). The bent region includes the modes 1 and 2. The intermediate region consists of modes 3, 4, and 5. The stretched region contains mode 6 and 7.

The bent region modes are observed only in DNA-systems. These modes are characterized by short distances between the ends of spermidine^{3+} molecule (Table 2) for which the repulsion between the positively charged atoms of polyamine is the highest. Therefore, modes 1 and 2 are characterized by relatively low intensity in the conformational spectra, especially mode 1 (Fig. 2). The interactions between positively charged polyamines with the negatively charged atoms of the double helix backbone stabilize the conformations of spermidine^{3+} molecules in modes 1 and 2. Therefore, these modes are observed only in the DNA-system, while in the system without DNA there are no peaks in this region of the conformational spectra.

The modes 3, 4, and 5 are present in spermidine^{3+} conformational spectra of both simulated systems and are rather intense. However, the positions of the maxima of modes 3 and 4 are slightly different in the two systems. Such a difference is related to the difference of the shape of the conformational spectra of polyamine in DNA-system and in solution-system. Differently from the DNA-system, the solution-system does not display maxima in the region of the conformational spectra < 9 Å. The lack of maxima in this region introduces some uncertainty in the position of Gaussians of modes 3 and 4 in the spectra of solution-system

Table 2
Mean values of end-to-end distances (Å) for each conformational mode of spermidine^{3+}, grouped in three regions.

	Bent region		Intermediate region			Stretched region	
System	Mode 1	Mode 2	Mode 3	Mode 4	Mode 5	Mode 6	Mode 7
DNA	4.71	6.67	7.69	8.99	9.85	10.53	11.34
Solution	–	–	8.76	9.31	9.85	10.53	11.34

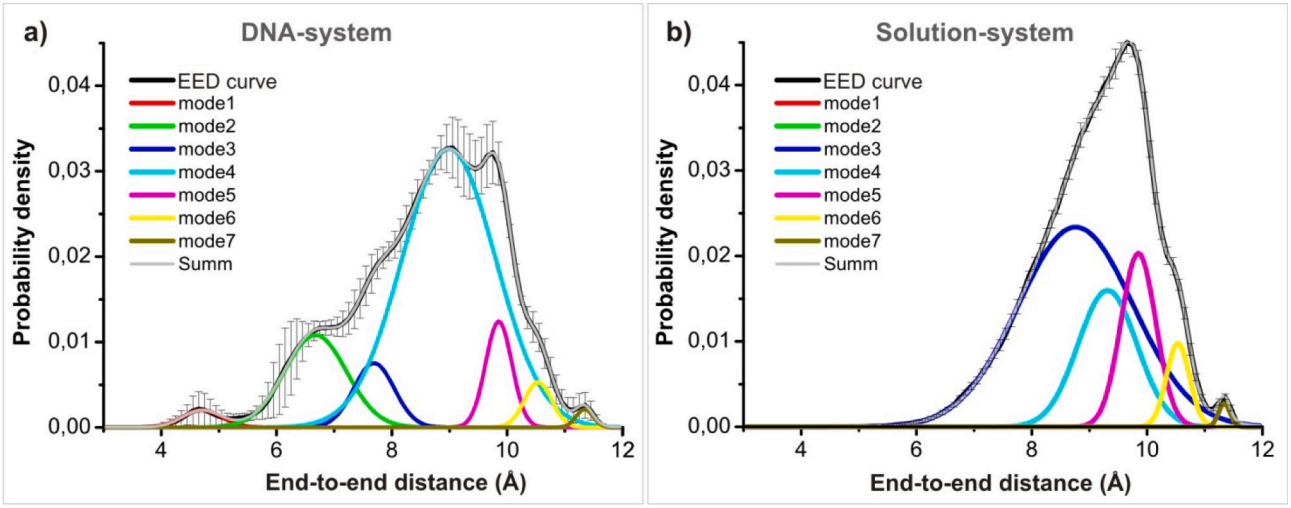

Fig. 2. Conformational spectra of spermidine^{3+} describing the distribution of the EED. The spectra are fitted by 7 Gaussian functions (modes), see text. a) The conformational spectra averaged over all spermidine^{3+} molecules and all trajectories of DNA-system (trajectories A, B, C, D and E). The error bars show standard deviations of different trajectories spectra. b) The conformational spectra averaged over all spermidine^{3+} molecules of the solution-system.

(Fig. 2b). The position of mode 5 is the same in both DNA- and solution-system (Fig. 2). The modes of this region are characterized by a high intensity, especially mode 4, which indicates that these modes represent the most probable conformational states of polyamine molecules.

Modes 6 and 7 form the stretched region of the conformational spectra of specrmidine^{3+}. The EED of these modes are close to the maximum length of the polyamine molecule. The positions of these modes are almost the same in the two simulated system types (Table 2). Mode 6 is observed as a shoulder, while mode 7 is characterized by a small but prominent peak (Fig. 2). The position of mode 7 corresponds to the maximally stretched state of spermidine^{3+} molecule, where all dihedral angles are close to the *trans* conformation.

To conclude this section, the analysis of the EEDs has led to the identification of seven distinct conformational modes for spermidine^{3+}. Two of the modes appear only in the DNA-system and the other five modes are present in both systems (i.e., with or without DNA).

3.2. Analysis of dihedral angles of spermidine^{3+}

The conformational modes of the polyamine molecules are adopted through variation in their backbone dihedral angles. Each of these dihedral angles can adopt three states (*gauche*$^{+/-}$ and *trans*). Different conformational states of the molecule are attained through different combinations of states of the dihedral angles. The flexible structure of positively charged spermidine^{3+} is useful to optimize the interactions with the negatively charged groups of the DNA double helix. Performing an analysis of the population of each combination of dihedral angles would help to better understand the structural heterogeneity within each mode.

The probability distribution for the dihedral angles was calculated for each polyamine, and then the average over the entire set of molecules in all the simulated systems was computed (Fig. 3). The dihedral angles are numerated with the Roman numbers I, II, III, IV, V, VI, and VII starting from a terminal atom N (Fig. 3 on the left). The error bars in the figures reflect the degree of variability around the average value across the values adopted during the simulations. The obtained distributions are rather symmetric within the range of error bars, especially in the case of the solution-system. Different dihedral angles are characterized by different intensities of the maxima in *gauche*$^{\pm}$ and *trans* states. The probabilities in these states ($P^D_{Gauche-}$,$P^D_{Gauche+}$ and P^D_{Trans}) were determined by integration of the maxima in the curves in Fig. 3, and are reported in Table 3.

The obtained probabilities are rather similar for the system with and without DNA. The dihedral angles II, IV and V are characterized by high

Table 3
Probability of occupation of *gauche* and *trans* states of dihedral angles in spermidine^{3+}, in the DNA-system (Solution-system). The values are indicated in %.

State	I	II	III	IV	V	VI	VII
trans	43.7 (42.0)	85.2 (85.8)	54.7 (53.3)	75.9 (77.3)	84.9 (80.4)	39.5 (54.7)	19.5 (29.0)
gauche-	25.0 (29.0)	7.8 (7.1)	19.2 (23.0)	12.0 (11.3)	7.9 (9.76)	29.0 (22.7)	40.2 (35.6)
gauche+	31.3 (29.0)	7.1 (7.1)	26.2 (23.7)	12.0 (11.4)	7.2 (9.82)	31.4 (22.6)	40.3 (35.4)

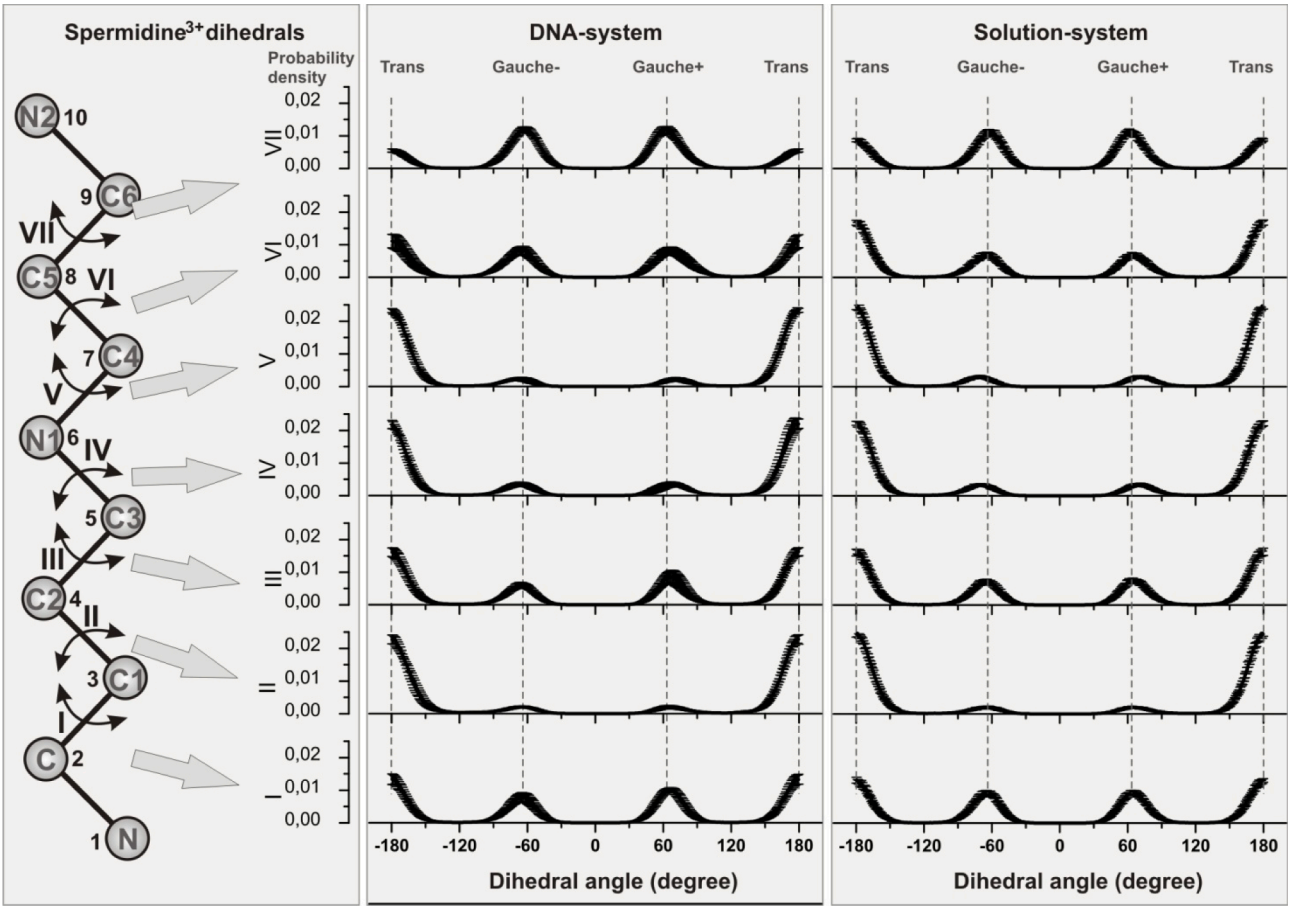

Fig. 3. Dependence of probability density of dihedral angles of spermidine^{3+} molecule backbone in the DNA-system and solution-system. The error bars appear as the results of averaging over all spermidine^{3+} molecules and all trajectories. The definition of the angles I, II, III, IV, V, VI, and VII for the backbone atoms of the molecule are shown on left.

probabilities of *trans* conformation and only about 10% of the time they can be in the *gauche*$^+$ or in the *gauche*$^-$ conformations. The dihedral angles I, III and VI still have rather high probabilities of *trans* state (from ~ 40% to ~ 50%), but in total these angles stay the same or even longer time in *gauche*$^{+/-}$ states. The dihedral angle VII is characterized by high probability to adopt *gauche*$^+$ and *gauche*$^-$ conformations compared to *trans* state, especially in the DNA-system. The *gauche*$^+$ and *gauche*$^-$ states display about equal occupation for all the dihedral angles in both systems, while the probability with respect to the *trans* state depends on the dihedral angle and is not affected by the presence of DNA.

Each dihedral angle of the polyamine molecule can occupy one of three states, and this is expressed by the following condition:

$$P^D_{Trans} + P^D_{Gauche} = 1\,, \tag{1}$$

where $P^D_{Gauche} = P^D_{Gauche-} + P^D_{Gauche+}$. Based on the similarity of (1) to the basic trigonometric equation $\sin^2\gamma + \cos^2\gamma = 1$, we can write:

$$\begin{aligned} P^D_{Trans} &= \sin^2\gamma\,, \\ P^D_{Gauche} &= \cos^2\gamma\,. \end{aligned} \tag{2}$$

Here the variable γ joins the probabilities of *gauche* and *trans* states. The range of γ is from 0 to $\pi/2$ and it may be written explicitly as $\gamma = \cos^{-1}(P^{1/2}_{Gauche})$ or the equivalent $\gamma = \sin^{-1}(P^{1/2}_{Trans})$. In the following analysis, the normalized variable $\widetilde{\gamma} = \gamma/(\pi/2)$, with the variation range from 0 to 1, will be used. The value $\widetilde{\gamma} = 1$ corresponds to the dihedral angle in the *trans* state, while the value $\widetilde{\gamma} = 0$ corresponds to the dihedral angle in one of the *gauche* states (*gauche*$^+$ or *gauche*$^-$) with 50% probability for each *gauche* state. In the present work the parameter $\widetilde{\gamma}$ is referred to as the combined conformational probability. The values of the combined conformational probabilities for the dihedral angles of spermidine^{3+} molecule are displayed in Fig. 4.

The results indicate that the dihedral angles of spermidine^{3+} are not uniformly distributed in the *trans* and *gauche* states. The dihedral angles II, IV and V are mostly in *trans*, while the dihedral angle VII is mostly in *gauche* states. The dihedral angles I, III and VI are characterized by the combined conformational probability about 0.5, indicating that these dihedral angles stay about equal time in *gauche* and *trans* states.

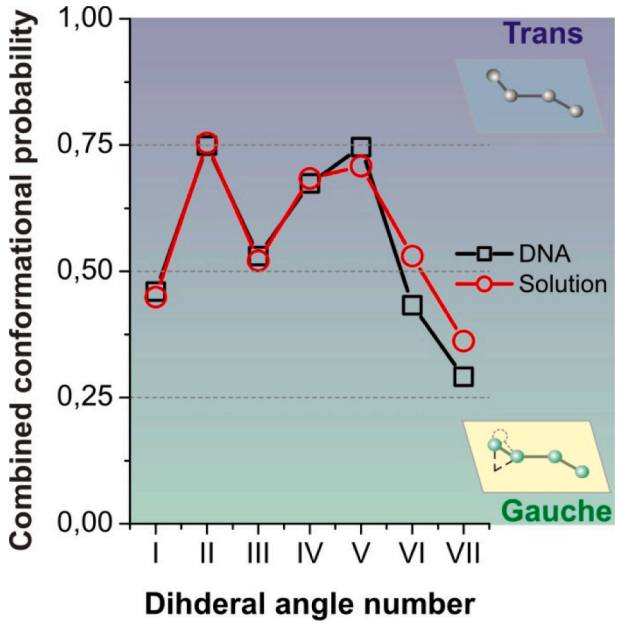

Fig. 4. The dependence of combined conformational probability ($\widetilde{\gamma}$) on the dihedral angle number of spermidine^{3+} molecule in the DNA- and solution-systems. $\widetilde{\gamma}$ increases as the probability of *gauche-trans* transition increases (see text for definition).

However, taking into consideration that there are two different *gauche* states (*gauche*$^+$ and *gauche*$^-$), the *trans* state still has higher occupancy in the case of I, III and VI dihedral angles. According to the value of the combined conformational probability, the dihedral angles can be arranged in the following order:

$$\widetilde{\gamma}_{VII} < \widetilde{\gamma}_{III}, \widetilde{\gamma}_{VI}, \widetilde{\gamma}_{I} < \widetilde{\gamma}_{II}, \widetilde{\gamma}_{V}, \widetilde{\gamma}_{IV}\,. \tag{3}$$

Taking into consideration that the conformational spectrum of spermidine^{3+}, consists of 7 modes (Fig. 2), the distribution of probability density for each dihedral angle has been analyzed for each mode. The results for the DNA system are shown in Fig. 5, and the results for the solution-system are shown in Supplemental Materials (Figure S6).

The results in Fig. 5 show that mode 7, characterizing the stretched conformation of spermidine^{3+}, consists of dihedral angles which are all in *trans* state. This is natural, since in mode 7 the EED is the sum of distances between the 1–4 atoms of each dihedral angle, which is the longest in the case of *trans* state. Mode 6 can be attained from mode 7 by the switching of the dihedral angles I and VII at the ends of the polyamine molecule from *trans* to *gauche* states. The occurrence of other dihedral angles in *gauche* state in the case of this mode is much lower. The *gauche*$^{+/-}$ peaks increase and *trans* peaks decrease as the EED of spermidine^{3+} decreases, as observed by the modes 5, 4, 3, 2, and 1 (Fig. 5). The exceptions are the dihedral angles II, IV and V, which stay mostly in *trans* conformation. Note, the dihedral angle II in the case of mode 1 is essentially distorted and the dependence of this angle is not typical.

Calculating the integrals below the maxima of the probability densities shown on the Fig. 5, the probabilities for each *trans* and *gauche* states of the dihedral angles have been determined for the DNA and solution systems (Fig. 6). The combined conformational probability was also calculated using formulae (2) and shown as the curve with "square dots" on the same histogram.

The data in Fig. 6 show that for the dihedral angles I, III, VI, and VII the probability of *trans* conformation gradually increases with increasing mode number (from mode 1 to mode 7) and so does the combined conformational probability. For the dihedral angles II and IV, the probability of *trans* state increases very slowly as the number of mode increases, starting from the probability higher than 0.5 in mode 1. In the case of dihedral angle V, the probability of the *trans* state slightly decreases as the mode number increases to the minimal value at the mode 5 and then increases again. Note that the minimum value is still very high (about 0.7), indicating that this dihedral angle when the molecule adopts mode 5 conformation, is mostly in *trans* state. Thus, the angles II, IV and V stay in *trans* state almost all the time, while the dihedral angles I, III, VI, and VII are mostly *trans* in stretched conformations (modes 6 and 7).

As observed analyzing the data in Fig. 5, the data in Fig. 6 also show that in mode 7 all dihedral angles are in *trans* state, and mode 6 is mostly due to dihedral angle I or VII in the *gauche* state. Similarly, mode 5 is attained with the dihedral angle I and VII in *gauche* state (which is much more favored than in mode 6) and with an increased contribution of the *gauche* state from the other dihedral angles, except dihedral angle II. The increased bending of the polyamine in mode 4 involves the *gauche* state mostly for dihedral angles I, VI, and VII, and to a lesser extent also IV, while the other dihedral angles mostly retain the *trans* state. The modes 2 and 3 can be formed by different combinations of *gauche*$^+$ and *gauche*$^-$ states of dihedral angles I, III, VI and VII with the angles II, IV and V in *trans* state.

Each mode in the conformational spectra corresponds to the set of *trans/gauche*$^{+/-}$ states of the dihedral angles of spermidine^{3+} molecule. To find the relation between EED and the dihedral angles of spermidine^{3+} the apparatus of the statistical theory of chained molecules [42] was used. The details are described in the Supplemental Materials (Sections S5). This analysis allowed us to match the conformational modes with the set of dihedral angles of spermidine^{3+} molecule (Supplemental Materials, Table S4). The results indicated that the

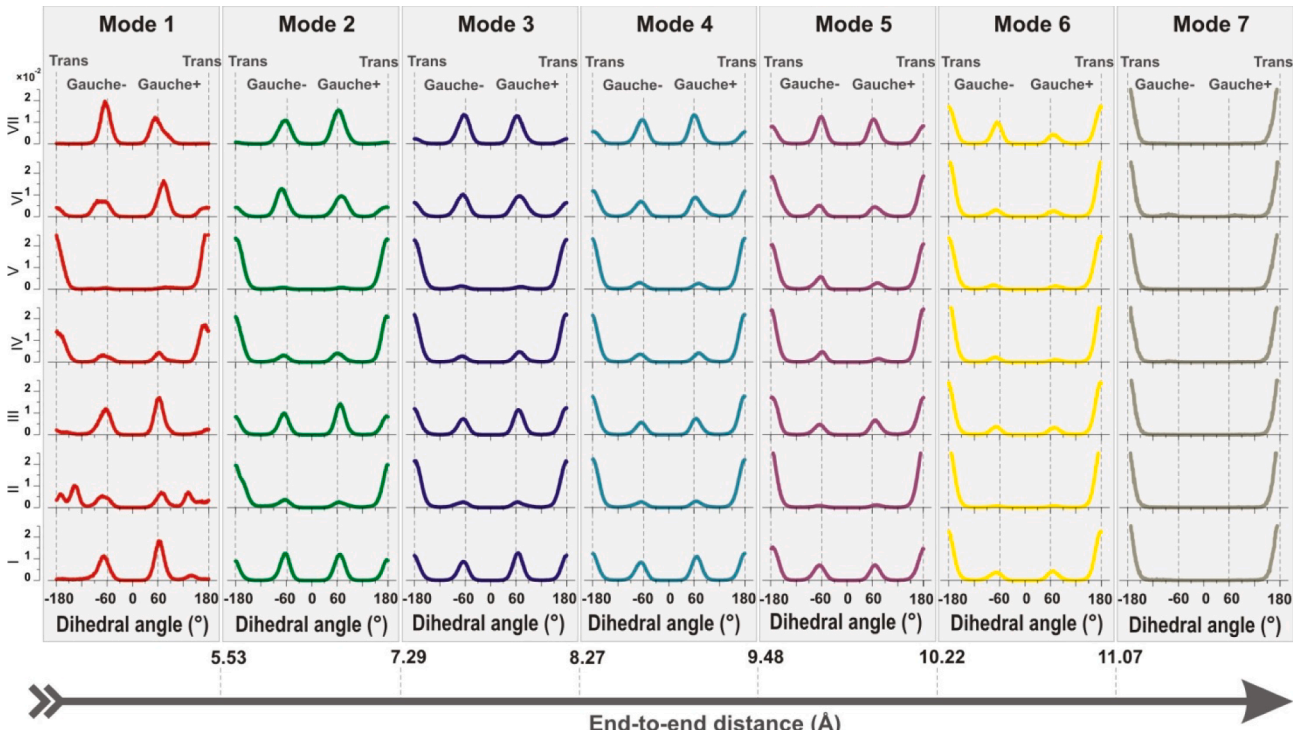

Fig. 5. Probability density of the dihedral angles of spermidine^{3+} for each mode of the conformational spectrum of DNA-system. The definition of the angles I, II, III, IV, V, VI, and VII as in Fig. 3. The EED distances reported at the bottom identify the limiting values for each of the seven conformational modes.

highest level of compaction of the polyamine, i.e., mode 1, is attained if the angles I, VI are in *gauche*$^+$ and the angles II, III, VII are in *gauche*$^-$ conformational states or *vice versa*. The values for the dihedral angles were taken from Table S2. The results show that only the angles IV and V are mostly in *trans* state. Note that in the case of mode 1 even the dihedral angle II, which is mostly in *trans* conformation, has a substantially increased probability to be in the *gauche* state compared to the other modes.

To recapitulate, the analysis described in this section indicates that while the bending of spermidine^{3+} molecule necessarily involves the *trans-gauche* conformational transition of some dihedral angles of the molecular backbone, the seven dihedral angles I-VII do not contribute to the same extent to the bending. The most external dihedral angles (I and VII) have a prominent role in the bending, followed by the dihedral VI and III. The probability of finding these dihedral angles in the *gauche* state gradually increases as the distance between end atoms of the molecule decreases. These four dihedral angles have a common feature: they all are N–C–C–C dihedral angles. The other dihedral angles, i.e., II, IV, and V which are either C–N–C–C or C–C–C–C dihedral angles, predominantly adopt the *trans* conformation even for small EED values. The preference of the *trans* conformation for the C–C–C–C dihedral angle of spermidine^{3+} molecule in water DNA solution is in agreement with the NMR data reported by Menger and D'Angelo. [43] In another NMR study, Maruyoshi et al. [44] observed that the conformational change of spermidine^{3+} when adding adenosine triphosphate in aqueous solution, are due to the increase of the gauche conformation of the N–C–C–C dihedral angles, in agreement with our simulations results. Thus, the molecular mechanism of spermidine^{3+} bending and binding involves mainly the *trans-gauche* conformational transitions of the N–C–C–C dihedral angles.

3.3. Analysis of energies of spermidine^{3+}

To rationalize the observation concerning the *trans-gauche* preferences described in the previous section, we analyzed the energy of the spermidine^{3+} conformations observed during the MD simulations.

To analyze the energetics of spermidine^{3+} the potential energies of each dihedral angle of the polyamine molecule has been calculated as a function of the dihedral angle value. The analysis was performed on the solution-system. Only intramolecular interactions between polyamine atoms are considered. All components of the force field energy (equation S1 in Supplemental Materials) have been analyzed individually as a function of the value of the dihedral angles: the energy of bonds, the energies of valence and dihedral angles, the energies of electrostatic and van der Waals interactions between the atoms involved in the dihedral angle and the other atoms of the polyamine molecule. To take into consideration the screening of electrostatic interactions by the solvent, a value of 80 was used as dielectric constant in the calculations of Coulombic interactions. A set of MD simulations of the system of spermidine^{3+} in implicit solvent (the results are not presented) have shown that such a value of dielectric constant is a good approximation for the description of the conformational properties of the polyamine molecule. In particular, the probability distributions for the dihedral angles of spermidine^{3+} molecule in implicit solvent with the dielectric constant 80 are qualitatively the same as in explicit solvent. Calculations have been carried out for each spermidine^{3+} molecule of the system and then averaged over all molecules. The details of the calculations are described in Supplemental Materials (Section S5).

The results displayed in Fig. 7a show that the energy of the bonds involved in the dihedral angle barely varies as the angle changes, owing to the small bond stretching that occurs with rotation.

The variation in the valence angles energy as the dihedral angle changes falls within the 2–3 kcal/mol range and increases gradually as the molecule transitions from 180° toward small angle values (see Fig. 7b).

The energy of the dihedral angles is characterized by the minima in *trans*, *gauche*$^+$ and *gauche*$^-$ states (Fig. 7c). The shape of the energy profile of the dihedral angle is the same as the shape of the potential functions of the force field (Figure S8). The values of the dihedral angle potential energy vary from 0 to 3 kcal/mol. The *trans* and *gauche* minima of the potential are equal, for all dihedral angles with exception of dihedral angle II which displays a lower minimum in *trans* state.

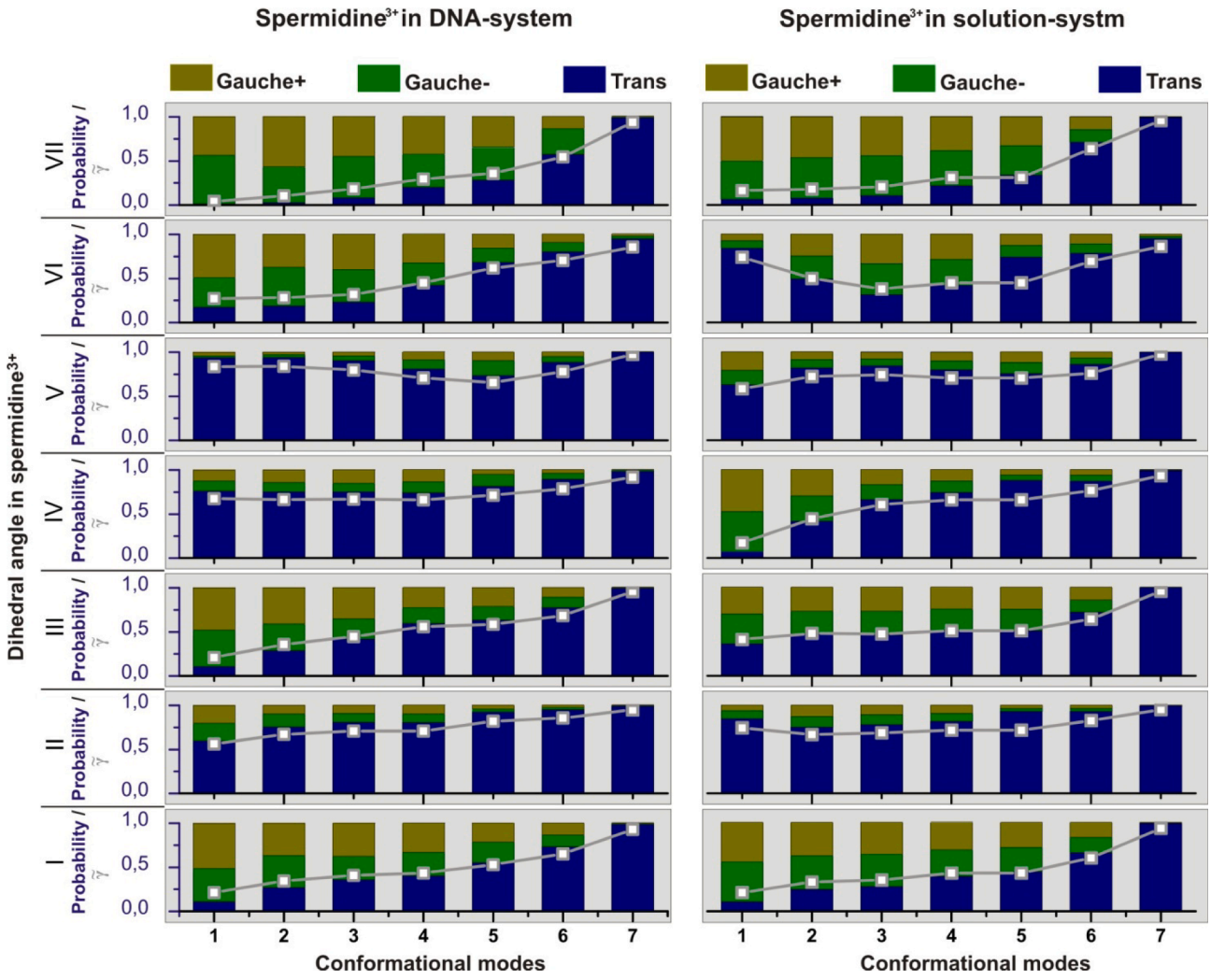

Fig. 6. Probabilities of *gauche* and *trans* states of the dihedral angles in spermidine^{3+}, for the seven conformational modes observed in the DNA-system and Solution-system. The histogram bars for *trans*, *gauche*$^{+}$ and *gauche*$^{-}$ state are shown in blue, dark yellow and olive colors, respectively. The combined conformational probabilities $\tilde{\gamma}$ are shown as grey line with squares. The scales for the histogram bars and combined conformational probabilities are the same and shown on the left in blue.

The dependence of the van der Waals interactions energy on the dihedral angle varies with the dihedral. For dihedral angles I, III, VI, and VII, prominent minima in *gauche* states and, hardly visible, minima in *trans* states are observed. For II, IV, and V, the minima in *gauche* and *trans* states are about equal. The van der Waals energies are always negative, ranging from −3 to −6 kcal/mol.

The energies of electrostatic interactions are always positive (repulsive) in the range from 1 to 3 kcal/mol and practically do not depend on the value of the dihedral angle.

The sum of all contributions to the total energy is within the range from −2 to 4 kcal/mol. In general, the total energy has the minima in *trans* and in *gauche*$^{\pm}$ states, following the trend of the potential energy of the dihedral angle. However, the depth of the potential wells is different. The *trans* and *gauche* minima are not equal, making it somewhat difficult to characterize the dependence of the energy of the dihedral angle on the angle value. To characterize the difference between different dihedral angles the potential barriers between *trans* and *gauche* states have been analyzed (Table 4).

Data in Table 4 show that the *trans-gauche* (ΔE_{T-G}) and *gauche-trans* (ΔE_{G-T}) potential barriers are different. This difference, $\Delta\Delta E = \Delta E_{G-T} - \Delta E_{T-G}$, is positive for angles I, III, VI, and VII, and negative for II, IV, and V. The positive (negative) difference of potential barriers means that the number of *trans-gauche* (*gauche-trans*) jumps will be higher than *gauche-trans* (*trans-gauche*) jumps, and *gauche* (*trans*) state will be more prominent. The difference of the potential barriers may be arranged in the following order:

$$\Delta\Delta E_{II} < \Delta\Delta E_{V} < \Delta\Delta E_{IV} < \Delta\Delta E_{III} < \Delta\Delta E_{I} < \Delta\Delta E_{VI} < \Delta\Delta E_{VII} \quad (4)$$

The order in equation (4) above corresponds to the order of combined conformational probability equation (3), representing the occurrence of the dihedral angles in *gauche* and *trans* states.

Considering the above, we conclude that the calculated dependencies of the energy on the dihedral angle, explain the observed distribution of dihedral angles in the *gauche* and *trans* states.

3.4. Distribution and dynamics of spermidine^{3+} around the DNA double helix

To determine the influence of the DNA macromolecule on the conformational state of spermidine^{3+}, the correlation between EED of the polyamine molecule and localization around the double helix was calculated. The visual examination of the trajectories allowed selecting the characteristic snapshots for different conformational modes, shown in Fig. 8 and in the Supplemental Materials (Figure S9). Different conformations of spermidine^{3+} may be stabilized interacting with DNA in different regions of the double helix: minor groove, major grooves, and

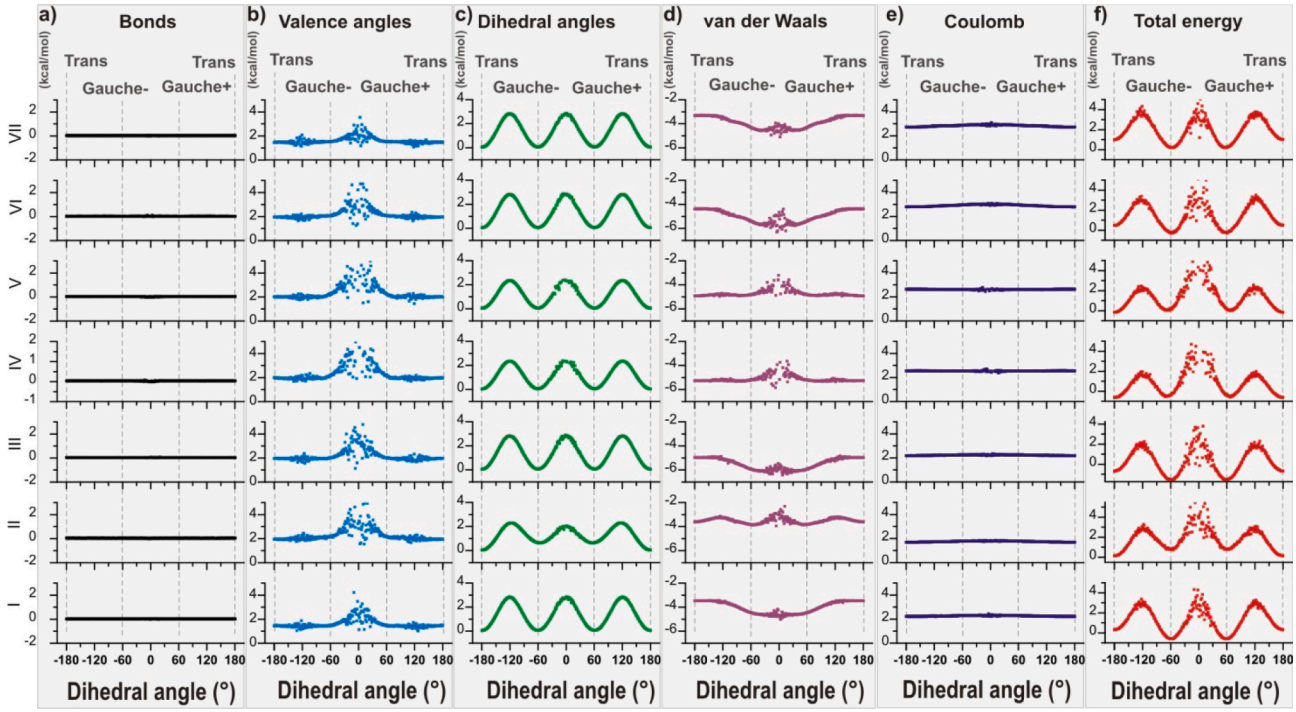

Fig. 7. Dependence of the spermidine^{3+} the potential energies of each dihedral angle of the polyamine molecule on dihedral angle value for the case of the solution-system. a) Energy of covalent bonds. b) Energy of valence angles. c) Energy of dihedral angles. d) Van der Waals energy. e) Electrostatic energy. f) Total energy (sum of all contributions).

Table 4
Potential barriers between *trans* and *gauche* states calculate from the total energy associated to each dihedral angle (kcal/mol). ΔE_{T-G} and ΔE_{G-T} are potential barriers of the transition from *trans* to *gauche*, and from *gauche* to *trans*, respectively; $\Delta\Delta E = \Delta E_{G-T} - \Delta E_{T-G}$ is the difference between potential barriers.

Potential barriers	I	II	III	IV	V	VI	VII
ΔE_{T-G}	2,83	3,10	2,94	2,52	2,61	2,89	3,05
ΔE_{G-T}	3,66	2,46	3,73	2,46	2,42	3,61	3,79
$\Delta\Delta E$	0,83	−0,64	0,79	−0,06	−0,18	0,72	0,74

the phosphate groups.

The conformational modes 1 and 2 of spermidine^{3+} are the most bent and are possible due to the interaction with the phosphate groups of the DNA double helix (Fig. 8). The polyamines bind to DNA from the minor groove side "hugging" two phosphates of different strands of the double helix. The distance between oxygen atoms of the phosphate groups becomes very short < 4 Å resulting in a significative narrowing of the DNA minor groove (Figure S10). Such width of the minor groove of the double helix is not typical for DNA macromolecule in water solution, and it is possible due to the interaction with highly charged polyamine molecule. On the other hand, these conformational states of the polyamine are very rare in systems without DNA.

The conformations of spermidine^{3+} with the EED in the range between 7 and 10 Å (i.e., modes 3, 4, and 5) are observed in different regions around DNA (Fig. 8). These polyamine conformational modes may be adopted when it is in complex with the phosphate groups, in the minor and major grooves of the double helix, or even outside the double helix. Modes 3 and 4 are the most favored both in complex with DNA and in the solution.

The modes 6 and 7 are stabilized by the interactions with the phosphate groups when the polyamine is localized partially or as a whole in the minor groove of the double helix.

Summing up, the formation of complexes of polyamines with DNA induces modification in the structural preference of both partners in the complex: the presence of the DNA double helix do not alter the conformational modes but modify the distribution among them. On the other hand, the polyamine can induce changes in the double helix structure that can play a significant role in different biological processes, where DNA and polyamines are involved.

Spermidine^{3+} molecules interacting with DNA exhibit different degrees of translational mobility along the double helix depending on their position. Fig. 9 shows simulation snapshots illustrating the typical mobility of spermidine^{3+} molecules located in the DNA minor and major groups and at the phosphate backbone over a 750-ns trajectory. Inspection reveals that spermidines located in the minor and major grooves (e.g., red and blue colored molecules in Fig. 9) remain effectively at their initial positions over hundreds of nanoseconds, with typical movements of up to 1–2 neighboring base pairs. Those interacting with the phosphate groups (e.g., yellow molecule in Fig. 9) are more mobile, often moving ~ 5 base pairs; in exceptional cases, such phosphate-bound spermidine^{3+} molecules can traverse greater distances and even temporarily dissociate from DNA, moving freely in solution on the 10-ns timescale before returning to a new DNA binding site. However, on average the majority of spermidine^{3+} molecules bound to DNA move <3 base pairs along the double helix during the entire production phase of the simulations.

To characterize the proximity between polyamines in the DNA-system, the relative distribution of spermidine^{3+} molecules has been studied using the radial distribution functions (RDFs). The RDFs were

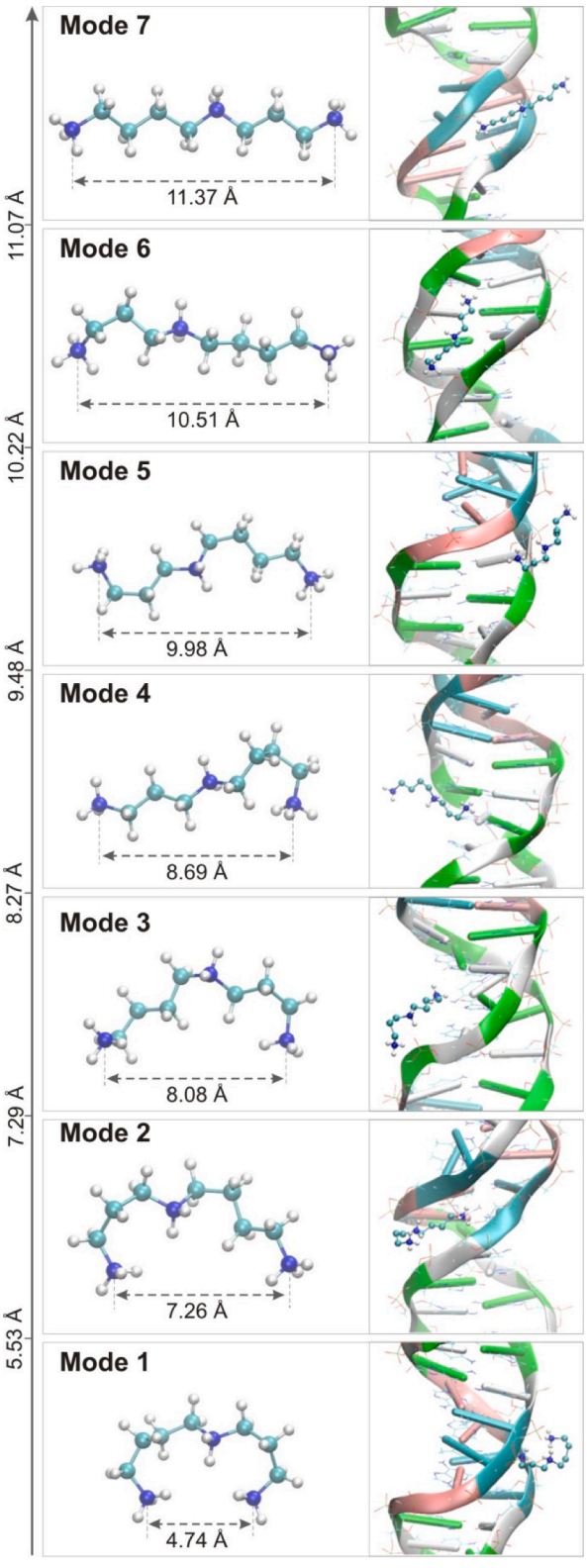

Fig. 8. Snapshots of spermidine^{3+} in different regions around the DNA double helix. The polyamine conformational modes are shown on the left omitting the DNA structure, and on the right the same conformation is shown in the environment where it is adopted. The snapshots of spermidine^{3+} shaped in different regions of the DNA double helix are shown on the right. The numerical scale on the left indicates the limiting EED used to discriminate between the conformational modes.

calculated separately for each atom in the backbone of spermidine^{3+} with respect to all the atoms of the backbone of the other spermidine^{3+} molecules in DNA-system (Figure S11). The analysis of the RDFs and of their integrals indicate that the closest distance is about 5 Å. However, such distances are relatively rare, as expected because of the repulsion between the positively charged amino groups, and the mean value of the distance between polyamine atoms is typically within the range from 6.5 Å to 9.5 Å (Figure S12). The smallest values for this distance are observed for the atoms at the ends of spermidine^{3+} backbone, indicating that the favorite arrangements of the polyamines relative to each other have the terminal parts close to each other. Interestingly, the C2 atoms display the largest coordination at short distances, hinting on a possible role of the difference in the length of the carbon chains (one having four C atoms and the other 3), to optimize their interactions.

4. Discussion and conclusions

Natural polyamine such as putrescine^{2+}, spermidine^{3+}, and spermine^{4+} [1] can exhibit a large number of different conformations due to the presence of many rotatable bonds in their molecular backbone. In the present work, for the first time, a comprehensive study of the conformational space of spermidine^{3+} has been carried out based on atomistic MD simulations in aqueous solution, with and without a double stranded DNA. Analyzing the end-to-end distances of the polyamine, the 2187 possible chain conformations have been grouped in 7 distinct families. The number of conformational families corresponds to the number of dihedral angles in the polyamine backbone and is the same both in water solution and when interacting with DNA double helix. However, the relative probability of each conformational mode is highly affected by the presence of DNA. In particular, compact conformations that are very rare in the solution become relevant in the DNA-polyamine system.

To elucidate the structural effects related to the complex formation, the dihedral angles of the spermidine^{3+} molecule have been analyzed. The results show that three of seven dihedral angles are mostly in *trans* conformation during the entire set of simulations, while other 4 dihedral angles can switch to the *gauche*$^{+}$ or *gauche*$^{-}$ depending on the mode. The energy analysis showed that the driving force beyond the distribution among the dihedral angles, either *trans* or *gauche*, is mainly determined by the corresponding dihedral angle potential and van der Waals interactions. The other terms of the potential energy (bonds, valence angle and electrostatic interactions) do not contribute significantly to the variation of the potential energy with the dihedral angle. In particular, varying the dihedral angle the electrostatic interactions provide a constant repulsive contribution due to the positively charged amino groups.

In the presence of DNA, different conformations of spermidine^{3+} are stabilized by the interactions with the negatively charged phosphate groups. The analysis of the correlations between polyamine conformations and their localization in proximity of the double helix reveals that spermidine^{3+} adopts different conformational modes in different regions of DNA. The polyamines that are entirely localized in the minor groove display stretched conformations, adopting the shape of the chains of the phosphate backbones. In the major groove, the polyamines adopt structures with intermediate bending. The conformational states with the shortest end-to-end distances are those characterized by the polyamine "hugging" the negatively charged phosphate groups, hence located outside the grooves of DNA double helix. These modes are characteristic for the DNA-polyamine system and are rarely observed in aqueous solution in the absence of DNA.

Overall, our results shed light on the rich conformational variability of polyamines. The obtained results can be also useful for designing and building up coarse grained models tailored to DNA-polyamine systems to be used in large scale simulations. In view of these outcomes, it would be interesting to extend the present investigation to the study of the dependence of the spermidine^{3+} conformations on its concentration. Furthermore, considering the importance of polyamines in the

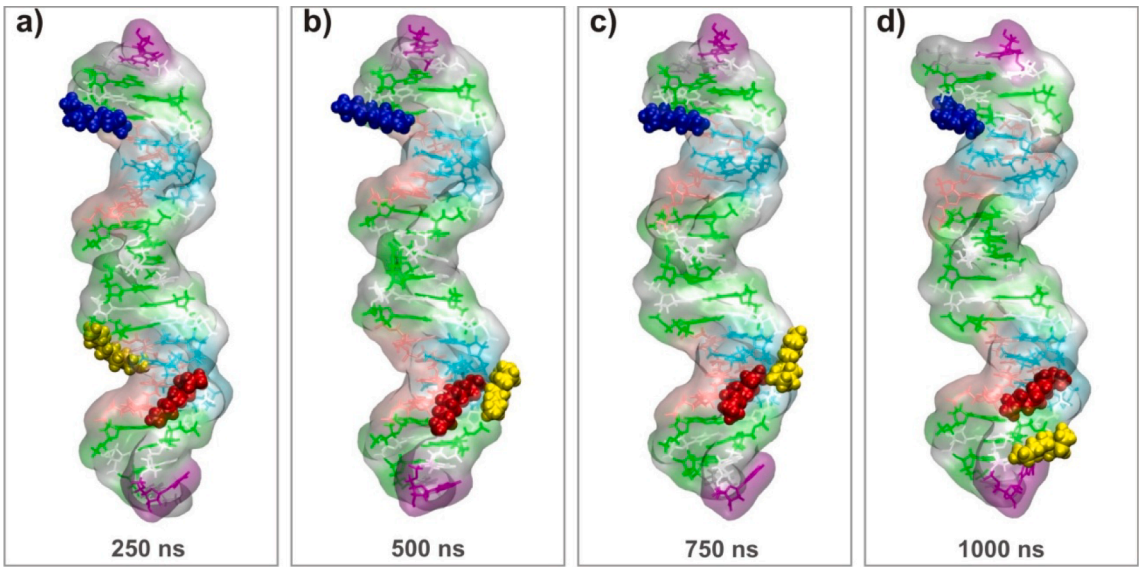

Fig. 9. Representation of the mobility of spermidine^{3+} around DNA during 1-μs simulation. Three spermidine molecules are shown, with initial locations (a, 250 ns) in the minor (red), major (blue), and at the phosphate backbone (yellow). Snapshot labels and corresponding simulation times: a) 250 ns; b) 500 ns; c) 750 ns; d) 1000 ns. Spermidine^{3+} molecules are shown using a space filling ("VdW") representation and color coded. For DNA, a transparent surface representation is superimposed on a line representation using the same residue-based color scheme employed in the other figures.

condensation of DNA, their behavior in proximity to other different macromolecules (e.g., RNA and proteins) should also be analyzed. Finally, the proposed approach applied in the study of the conformational space of spermidine^{3+} can be easily applied to other natural polyamines, for example, spermine^{4+}, putrescine^{2+}, cadaverine^{2+}, thus highlighting similarities and differences in their interaction modes to be connected to their biological activity.

CRediT authorship contribution statement

Sergiy Perepelytsya: Conceptualization, Methodology, Validation, Formal analysis, Writing – original draft, Writing – review & editing, Project administration. **Tudor Vasiliu:** Formal analysis, Data curation, Methodology, Investigation, Writing – original draft, Writing – review & editing. **Aatto Laaksonen:** Supervision, Resources, Funding acquisition, Writing - review & editing. **Leon De Villiers Engelbrecht:** Visualization, Investigation, Conceptualization, Writing – review & editing. **Giuseppe Brancato:** Writing – review & editing. **Francesca Mocci:** Supervision, Conceptualization, Methodology, Writing - original draft, Writing - review & editing.

Declaration of Competing Interest

The authors declare that they have no known competing financial interests or personal relationships that could have appeared to influence the work reported in this paper.

Data availability

Data will be made available on request.

Acknowledgments

SP gratefully acknowledges the support from the National Academy of Sciences of Ukraine (project 0123U102290). All the authors acknowledge the COST Action CA21101 "Confined molecular systems: from a new generation of materials to the stars" (COSY) supported by COST (European Cooperation in Science and Technology). This paper is supported by European Union's Horizon Europe research and innovation programme under grant agreement No 101086667, project BioMat4CAST (BioMat4CAST - "Petru Poni" Institute of Macromolecular Chemistry Multi-Scale In Silico Laboratory for Complex and Smart Biomaterials). AL acknowledges financial support from the Swedish Research council (VR grant 2019-03865). Computer resources and technical support provided by PDC via Swedish National Infrastructure for Computing (SNIC grant 2022/5-601) at PDC are gratefully acknowledged.

Appendix A. Supplementary data

Supplementary data to this article can be found online at https://doi.org/10.1016/j.molliq.2023.122828.

References

[1] W. Saenger, Principles of Nucleic Acid Structure, Springer-Verlag, New York, 1984.
[2] Y.P. Blagoi, V.L. Galkin, V.L. Gladchenko, S.V. Kornilova, V.A. Sorokin, A. G. Shkorbatov, The Complexes of Nucleic Acids and Metals in the Solutions, Naukova Dumka, Kyiv, 1991.
[3] V.I. Maleev, M.A. Semenov, A.I. Gasan, V. A. Kashpur, Physical Properties of the DNA-Water System, Biofizika.
[4] A.A. Kornyshev, D.J. Lee, S. Leikin, A. Wynveen, Structure and interactions of biological helices, Rev. Modern Phys. 79 (2007) 943.
[5] Y.P. Blagoi, O.N. Veselkov, S. Volkov, D. Hovorun, M. Yevstigneev, R.O. Zhurakivsky, O.I. Korneliuk, V.Y. Maleev, M.O. Semenov, V.O. Sorokin, V.M. Kharkianen, C.L.M., A.V. Shestopalova, Physical Principles of Molecular Organization and Structural Dynamics of Biopolymers (V. N. Karazin Kharkiv National University, Kharkov, 2011).
[6] F. Mocci, A. Laaksonen, Insight into nucleic acid counterion interactions from inside molecular dynamics simulations is "Worth Its Salt", Soft Matter 8 (2012) 9268.
[7] R. Lavery, J.H. Maddocks, M. Pasi, K. Zakrzewska, Analyzing ion distributions around DNA, Nucl. Acids Res. 42 (2014) 8138.
[8] M. Pasi, J.H. Maddocks, R. Lavery, Analyzing ion distributions around DNA: sequence-dependence of potassium ion distributions from microsecond molecular dynamics, Nucleic Acids Res. 43 (2015) 2412.
[9] P.D. Dans, L. Danilane, I. Ivani, T. Drsata, F. Lankas, A. Hospital, J. Walther, R. I. Pujagut, F. Battistini, J.L. Gelpi, R. Lavery, M. Orozco, Long-timescale dynamics of the drew-dickerson dodecamer, Nucleic Acids Res. 44 (2016) 4052.
[10] S. Perepelytsya, Hydration of counterions interacting with DNA double helix: a molecular dynamics study, J. Mol. Model. 24 (2018) 171.
[11] S. Perepelytsya, J. Uličný, A. Laaksonen, F. Mocci, Pattern preferences of DNA nucleotide motifs by polyamines putrescine2+, spermidine3+ and spermine4, Nucleic Acids Res. 47 (2019) 6084.
[12] F. Mocci, A. Laaksonen, L. Engelbrecht, T. Vasiliu, S. Perepelytsya, DNA-polyamine interactions: insight from molecular dynamics simulations on the sequence-specific binding of spermidine3+, in: Soft Matter Systems for Biomedical Applications. Springer Proceedings in Physics, 266, Springer, Cham, 2022, pp. 163–192.

[13] T. Vasiliu, F. Mocci, A. Laaksonen, L.D.V. Engelbrecht, S. Perepelytsya, Caging polycations: effect of increasing con Fi nement on the modes of interaction of Spermidine3+ With DNA double helices, Front. Chem. 10 (2022) 1.
[14] V.A. Bloomfield, D.N.A. Condensation, Curr. Opin. Struct. Biol. 6 (1996) 334.
[15] N. Korolev, A.P. Lyubartsev, L. Nordenskiöld, A. Laaksonen, Spermine: an "Invisible" component in the crystals of B-DNA. A grand canonical Monte Carlo and molecular dynamics simulation study, J. Mol. Biol. 308 (2001) 907.
[16] N. Korolev, A.P. Lyubartsev, A. Laaksonen, L. Nordenskiöld, On the competition between water, sodium ions, and Spermine in binding to DNA: a molecular dynamics computer simulation study, Biophys. J . 82 (2002) 2860.
[17] N. Korolev, A.P. Lyubartsev, A. Laaksonen, L. Nordenskiöld, A Molecular dynamics simulation study of polyamine- and sodium-DNA. Interplay between polyamine binding and DNA structure, Eur. Biophys. J. 33 (2004) 671.
[18] G. Iacomino, G. Picariello, L. D'Agostino, DNA and nuclear aggregates of polyamines, Biochim. Biophys. Acta - Mol. Cell Res. 1823 (2012) 1745.
[19] E. Bignon, C.H. Chan, C. Morell, A. Monari, J.L. Ravanat, E. Dumont, Molecular dynamics insights into polyamine–DNA binding modes: implications for cross-link selectivity, Chem. - A Eur. J. 23 (2017) 12845.
[20] J. Yoo, H. Kim, A. Aksimentiev, T. Ha, Direct evidence for sequence-dependent attraction between double-stranded DNA controlled by methylation, Nat. Commun. 7 (2016) 1.
[21] J. Yoo, A. Aksimentiev, The structure and intermolecular forces of DNA condensates, Nucleic Acids Res. 44 (2016) 2036.
[22] A.A. Ouameur, H.A. Tajmir-Riahi, Structural analysis of DNA interactions with biogenic polyamines and cobalt(III)hexamine studied by fourier transform infrared and capillary electrophoresis, J. Biol. Chem. 279 (2004) 42041.
[23] K. Igarashi, K. Kashiwagi, Modulation of cellular function by polyamines, Int. J. Biochem. Cell Biol. 42 (2010) 39.
[24] M.M. Patel, T.J. Anchordoquy, Ability of spermine to differentiate between DNA sequences-preferential stabilization of A-tracts, Biophys. Chem. 122 (2006) 5.
[25] A. Kabir, G. Suresh Kumar, Binding of the biogenic polyamines to deoxyribonucleic acids of varying base composition: base specificity and the associated energetics of the interaction, PLoS One 8 (2013) e70510.
[26] M.A. Keniry, Æ.E.A. Owen, An investigation of the dynamics of spermine bound to duplex and quadruplex DNA by 13 C NMR, Spectroscopy 637 (2007).
[27] K. Maruyoshi, K. Nonaka, T. Sagane, T. Demura, T. Yamaguchi, N. Matsumori, T. Oishi, and M. Murata, Conformational Change of Spermidine upon Interaction with Adenosine Triphosphate in Aqueous Solution, 1618 (2009).
[28] D. A. Case, I. Y. Ben-Shalom, S. R. Brozell, D. S. Cerutti, T. E. I. Cheatham, V. W. D. Cruzeiro, T. A. Darden, R. E. Duke, D. Ghoreishi, M. K. Gilson, H. Gohlke, A. W. Goetz, D. Greene, R. Harris, N. Homeyer, Y. Huang, S. Izadi, A. Kovalenko, T. Kurtzman, T. S. Lee, S. LeGrand, P. Li, C. Lin, J. Liu, T. Luchko, R. Luo, D. J. Mermelstein, K. M. Merz, Y. Miao, G. Monard, C. Nguyen, H. Nguyen, I. Omelyan, A. Onufriev, F. Pan, R. Qi, D. R. Roe, A. Roitberg, C. Sagui, S. Schott-Verdugo, J. Shen, C. L. Simmerling, J. Smith, R. S.- Ferrer, J. Swails, R. C. Walker, J. Wang, H. Wei, R. M. Wolf, X. Wu, L. Xiao, D. M. York, and P. A. Kollman, AMBER 2018, University of California, San Francisco.
[29] M.D. Hanwell, D.E. Curtis, D.C. Lonie, T. Vandermeersch, E. Zurek, G.R. Hutchison, Avogadro: an advanced semantic chemical editor, visualization, and analysis platform, J. Cheminform. 4 (2012) 17.
[30] Avogadro: An Open-Source Molecular Builder and Visualization Tool. Version 1.2.
[31] I. Ivani, P.D. Dans, A. Noy, A. Pérez, I. Faustino, A. Hospital, J. Walther, P. Andrio, R. Goñi, A. Balaceanu, G. Portella, F. Battistini, J.L. Gelpí, C. González, M. Vendruscolo, C.A. Laughton, S.A. Harris, D.A. Case, M. Orozco, Parmbsc1: a refined force field for DNA simulations, Nat. Methods 13 (2016) 55.
[32] J. Wang, R.M. Wolf, J.W. Caldwell, P.A. Kollman, D.A. Case, Development and testing of a general amber force field, J. Comput. Chem. 25 (2004) 1157.
[33] W.L. Jorgensen, J. Chandrasekhar, J.D. Madura, R.W. Impey, M.L. Klein, Comparison of simple potential functions for simulating liquid water, J. Chem. Phys. 79 (1983) 926.
[34] I.S. Joung, T.E. Cheatham, Determination of alkali and halide monovalent ion parameters for use in explicitly solvated biomolecular simulations, J. Phys. Chem. B 112 (2008) 9020.
[35] M.J. Abraham, T. Murtola, R. Schulz, S. Páll, J.C. Smith, B. Hess, E. Lindahl, GROMACS: high performance molecular simulations through multi-level parallelism from laptops to supercomputers, SoftwareX 1–2 (2015) 19.
[36] S. Nosé, A molecular dynamics method for simulations in the canonical ensemble, Mol. Phys. 52 (1984) 255.
[37] W.G. Hoover, Canonical dynamics: equilibrium phase-space distributions, Phys. Rev. A 31 (1985) 1695.
[38] M. Parrinello, A. Rahman, Polymorphic transitions in single crystals: a new molecular dynamics method, J. Appl. Phys. 52 (1981) 7182.
[39] B. Hess, H. Bekker, H.J.C. Berendsen, J.G.E.M. Fraaije, LINCS: a linear constraint solver for molecular simulations, J. Comput. Chem. 18 (1997) 1463.
[40] U. Essmann, L. Perera, M.L. Berkowitz, T. Darden, H. Lee, U. Essmann, L. Perera, M.L. Berkowitz, T. Darden, H. Lee, L.G. Pedersen, A smooth particle mesh ewald method, J. Chem. Phys. 103 (1995) 8577.
[41] W. Humphrey, A. Dalke, K. Schulten, VMD: visual molecular dynamics, J. Mol. Graph. 14 (1996) 33.
[42] P.J. Flory, Statistical Mechanics of Chain Molecules, Oxford University Press, 1969.
[43] F.M. Menger, L.L. D'Angelo, Conformation of DNA-bound spermidine by double 13C labeling, J. Org. Chem. 56 (1991) 3467.
[44] K. Maruyoshi, K. Nonaka, T. Sagane, T. Demura, T. Yamaguchi, N. Matsumori, T. Oishi, M. Murata, Conformational change of spermidine upon interaction with adenosine triphosphate in aqueous solution, Chem. - A Eur. J. 15 (2009) 1618.